

Exotic spintronic properties of transition-metal monolayers on graphyne

Xiaoxiong Ren,[†] Junsheng Huang,[†] Ping Li,[†] Yun Zhang,^{||} and Zhi-Xin Guo^{,†,§}*

[†]State Key Laboratory for Mechanical Behavior of Materials, Center for Spintronics and Quantum System, School of Materials Science and Engineering, Xi'an Jiaotong University, Xi'an, Shaanxi, 710049, China.

^{||}Department of Physics and Information Technology, Baoji University of Arts and Sciences, Baoji 721016, China.

[§]Key Laboratory of Polar Materials and Devices, Ministry of Education.

KEYWORDS: Horizontal magnetic tunnel junction, Magnetic monolayer film, 2D magnets, Transition metal, Half-metal

ABSTRACT: The recent discovery of two-dimensional (2D) magnetic materials which are compound of transition metal (TM) with other elements, has opened new avenues for basic research on low-dimensional magnetism and potential applications in spintronics. To further explore new 2D magnets of pure TM is thus of an interesting topic. Based on the first-principles calculations, here we propose a strategy of obtaining monolayer TM magnets, i.e., depositing TM atoms on graphyne (Gy) which has proper hexagonal hollow geometry. We find that TM monolayer with perfect hexagonal geometry can be formed on Gy. The TM monolayer exhibits a wealth of physical properties in dependence of TM species, such as ferromagnetic and antiferromagnetic ground states, as well as intriguing semimetal and half-metal characteristics. We also find that the half-metal characteristics makes the monolayer TM have great potential applications in the horizontal magnetic tunnel junction (MTJ) devices, where the tunneling magnetoresistance can reach as high as 850000%. Our results provide a new framework for obtaining 2D magnets with outstanding spintronic properties.

Two-dimensional (2D) magnetic materials can exhibit many novel physical properties which are of particular useful in the spintronics.¹⁻⁵ In the past decades, magnetic 2D materials were usually created in an extrinsic way, e.g. defect engineering⁶⁻¹⁷ on non-magnetic 2D materials. Until recently, the discovery of 2D van der Waals (vdW) materials with intrinsic magnetism opens a new avenue to the 2D magnets. The interplay of dimensionality, correlation, charge, orbital character, and topology makes 2D magnetic crystals and heterostructures extremely fertile condensed matter systems with a large reservoir of exotic properties, such as quantum anomalous hall effect,¹⁸⁻²¹ unique spin-orbit coupling effect,^{22, 23} strong tunneling magnetoresistance (TMR) effect^{4, 24} and so on. These fascinating properties make them have great potential applications in the future spintronics.

At present, most studies focus on 2D magnetic materials composed of multiple compounds of transition metal (TM) and other elements, e.g. CrI_3 ,²⁵ MnBi_2Te_4 ²⁶ and Fe_3GeTe_2 ²⁷ and so on. Despite the fascinating properties of these 2D magnetic materials, the appearance of multiple element components easily induces defects such as uneven distribution of components and structures²⁸⁻³¹ during the synthesis process, which severely limits their wide application in spin-polarized devices. Therefore, it is greatly disable to find a way to obtain 2D magnetic material composed of pure TM.

On the other hand, the TM magnetic films such as Co, Fe are the mostly used magnetic materials in the present spintronic devices.³²⁻³⁴ In order to meet the development needs of miniaturization and high performance of spintronic devices, many methods had been proposed to further reduce the thickness of TM magnetic film³⁵⁻³⁷ as well as to synthesize them on a semiconductor substrate.³⁸⁻⁴⁰ However, owing to the agglomeration nature of TM atoms and the complex surface structure of semiconductor, it is extremely hard to obtain an atomic-thick magnetic TM film on the semiconductor substrates.

Here we propose that the 2D magnetic material can be obtained by depositing TM atoms on Gy which has a hexagonal hollow geometry. The deposited TM atoms prefer to locate on the hollow site of Gy and form a perfect honeycomb monolayer. We find several TM elements such

as V that are non-magnetic (NM) in their bulk phases have AFM ground state in their 2D structure, while the usually believed FM materials such as Ni presents NM ground state. The variation of magnetism can be attributed to the combined effects of out-of-plane symmetry broken and orbital hybridization with Gy. We also find that Nb, Mo exhibit the 2D half-metal characteristic, where the tunneling magnetoresistance in the magnetic tunnel junction (MTJ) is estimated as high as 850000%.

The first-principles calculations were performed by using the density functional theory (DFT)-based Vienna ab initio simulation package (VASP).^{41, 42} The ion–electron interaction was treated by the projector augmented-wave (PAW) technique.^{43, 44} Exchange–correlation energies were taken into account by the generalized gradient approximation (GGA) using the Perdew–Burke–Ernzerhof functional.⁴⁵ For TM monolayer, periodic boundary condition for the 2D structure was used, and a vacuum layer of 15 Å was set to avoid interactions in the out-of-plane direction. A plane wave basis set with a cutoff energy of 450 eV was used, and the first Brillouin-zone integration was carried out by a 15×15×1 Γ -centered Monkhorst-Pack grid.⁴⁶ Both of the atomic positions and lattice constants were optimized using a conjugate gradient method with criteria of energy and Hellmann–Feynman force convergence being less than 10⁻⁶ eV per unit cell and 0.01 eV Å⁻¹, respectively.

As for the calculation of tunneling magnetoresistance in the MTJ, we first optimized the atomic positions using a conjugate gradient method with criteria of energy and Hellmann–Feynman force convergence being less than 10⁻⁵eV per unit cell and 0.02 eV Å⁻¹, respectively. Then we constructed the MTJ device model as shown in [Figure 4a](#). The transmission calculations were carried out using the Atomistic Simulation Toolkit (ATK) with the PBE pseudopotentials distributed in the QuantumWise package.^{47, 48} The transmission is calculated using the non-equilibrium Green’s function (NEGF) approach.⁴⁹ A Gy/W/Gy supercell is used as the scattering region, ideally attached on both sides to semi-infinite Gy/Mo leads.^{50, 51} The Dirichlet boundary condition in the c-direction and periodic boundary conditions in the a-b plane were used in the simulation ([Figure 4a](#)). In the calculations, the Brillouin-zone of leads was sampled using

10×1×100 k points in the a, b, and c directions, respectively. Moreover, the NEGF–DFT self-consistency was controlled by a numerical tolerance of 10⁻⁵ eV.

We have considered γ -Gy as the substrate, which consists of hexagonal carbon rings and acetylene linkages, with 6 C atoms forming the $C_{sp} \equiv C_{sp}$ hybridization and the remaining 6 C atoms forming the $C_{sp^2} - C_{sp}$ hybridization, respectively.⁵²⁻⁵⁵ Our DFT calculations show that the lattice constant of freestanding Gy is 6.890 Å, agree with previous studies.⁵⁶⁻⁵⁸ We first systematically explored the stable geometries of the entire TMs from 3d to 5d on Gy. A common feature is that all the TM atoms prefer to locate on the hollow site above the center of acetylenic ring, where the monolayer TM with graphene-like structure can be formed in a proper coverage (Figure 1a). In addition, the nearest-neighbor distances between two TM atoms are around 3.8 Å, which is about 30% larger than atomic diameters of TM elements, meaning the nature of bonding interaction between two TM atoms. As discussed below, this feature can lead to strong Heisenberg exchange interaction and thus the FM phase of TM monolayers. On the other hand, the strong interface interaction between the TM and C induces significant buckling of graphyne (d1 in Table. 1), the value of which depends on the specific TM element (highly related to the atomic radius).

To evaluate the stability, we calculated the cohesive energy E_c of monolayer TM on Gy which is defined as,⁵⁹

$$E_c = (E_{Gy} + N_{TM}\mu_{TM} - E_{tot})/N_{TM}$$

where E_{Gy} and E_{tot} are the total energies of Gy and Gy/TM, respectively. N_{TM} is the number of TM atoms on graphyne and μ_{TM} is the chemical potential of TM which is adopted as the energy of an isolated TM atom. The cohesive energy E_c is defined above is the energy gain to grow TM monolayer on the Gy surface. As shown in Table I and Table SI, E_c of all TM monolayers is above 2.0 eV except for five group I B and II B elements (Ag, Au, Zn, Cd, Hg) which have completely filled orbitals. Such E_c value is larger than that of a monolayer TM on metal substrate and that of a group-IV monolayer on TM substrate, both of which had been experimentally synthesized,⁶⁰⁻⁶² showing the possibility of experimental synthesis for the

monolayer TM. The dynamical stability of such system was also confirmed in our previous study for Gy/Hf via ab initio molecular dynamics (AIMD) simulations.⁶³

Table I. Lattice constants and structure information of the key research systems. *a* represents the lattice constants of the systems. *M* represents the magnetic moment of a single TM in the Gy/TM systems. The *d1* and *d2* represent the distance between the transition metal atomic layer and the first layer C and the distance between the two layers C, respectively. *E_c* represents the cohesive energy of TM monolayer on Gy.

System	<i>a</i> (Å)	<i>M</i> (μ_B /TM)	<i>d1</i> (Å)	<i>d2</i> (Å)	Bandgap (eV)	<i>E_c</i> (meV)
Gy/V	6.566	1.096	0.77	0.82	0.345	3.352
Gy/Nb	6.589	0.606	0.98	0.83	0.066	4.931
Gy/Ta	6.588	0.642	0.93	0.86	0.367	5.940
Gy/Cr	7.035	3.366	0.00	0.00	—	2.117
Gy/Mo	6.585	1.582	0.92	0.81	—	3.512
Gy/W	6.552	1.456	0.89	0.85	—	4.898
Gy/Mn	6.752	3.018	0.58	0.61	0.852	2.389
Gy/Tc	6.632	1.721	0.84	0.75	0.398	4.240
Gy/Re	6.586	1.521	0.84	0.80	0.135	3.992
Gy/Fe	6.905	2.380	0.40	0.30	—	3.379
Gy/Co	6.946	1.293	0.12	0.12	—	4.013

Figure 1b shows the ground states of TM monolayers on Gy in the form of an element periodic table. As one can see, TM monolayers present plentiful stable phases covering FM, AFM and NM. Note that all the FM and AFM phases are for TM elements of group III B-VIII B with partially filled *d* orbitals. We further define weak-FM (AFM) and strong-FM (AFM) phases for a FM (AFM) monolayer with magnetic moment smaller and larger than $0.5 \mu_B/\text{atom}$, respectively. As shown in Figure 1b, all the elements of group V B-VII B have a strong FM/AFM phase, whereas the ones of group III B, IV B and a part of group VIII B present the

weak-FM/AFM phase. It is noticed that only four of VIII B elements have FM or AFM phase, while the remaining five present the NM phase.

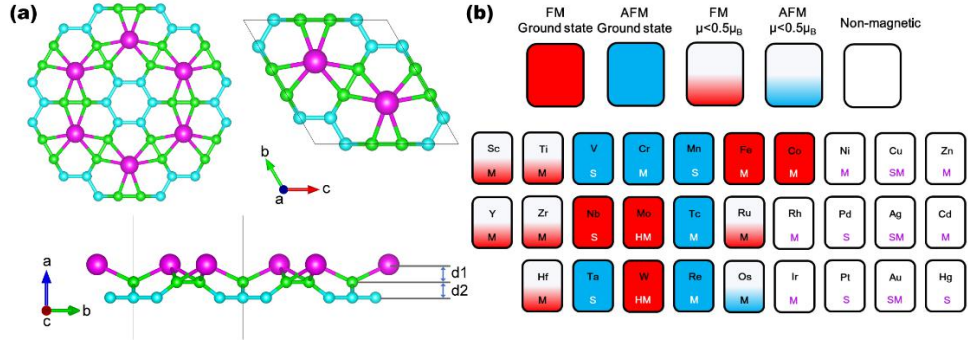


Figure 1. (Color online) Calculated structure and physical characteristics of Gy/TM system. (a) Hexagonal structure formed by TM in Gy/TM system (upper left), as well as the top view (upper right) and side view (lower) of a unit cell Gy/TM structure. The magenta, green, and blue atoms represent the TM atom, C atom in the nearest neighbor, and C atom in the next nearest neighbor to TM atom, respectively. d_1 and d_2 represent the distance between the TM atomic layer and the first layer C and the distance between the two layers C, respectively. (b) The physical properties of Gy/TM are given in the form of the periodic table, where the red, blue, and white background represent the magnetic ground states of ferromagnetic (FM), antiferromagnetic (AFM), and non-magnetic (NM), respectively. The full and partial filling of the background color represent that the magnetic moment of a single TM is greater than and less than $0.5\mu_B$, respectively. The letters S, M, HM and SM represent the properties of semiconductors, metals, half-metals and semimetals respectively.

In order to understand the origin of magnetism in TM monolayers, we carried out the d -orbital projection density of states (PDOS) analysis on TM atoms (Figure 2a-c). It is found that the split of energy levels of d orbitals (except for Fe and Mn as discussed below) basically present a triangular-prism-crystal-field (TPCF)-like distribution, i.e., the degenerate $d_{x^2-y^2}/d_{xy}$ orbitals, d_{z^2} orbital and degenerate d_{xz}/d_{yz} orbitals hold the energy levels from low to high energy, respectively. The formation of such TPCF-like distribution is a result of strong hybridization between d orbitals of TM atoms and p orbitals of the underlying C atoms as indicated in Figure S1, which significantly lowers the orbital symmetry of TM atoms compared to their bulk phases. This feature is confirmed by the calculated shortest TM–C distances (about 2.2 Å), which is comparable to the sum of the covalent atomic radii of TM and C atoms. Moreover, we find that the hybridization with p orbitals can help to fill the empty d orbitals by about two electrons per TM atom. Therefore, the variation of magnetism in the 2D structure can be owing to the strong p - d orbital hybridizations that induce significant orbital-symmetry

breaking and orbital filling, which are responsible for the distribution of spin-up and spin-down electrons in the crystal field. Considering that both the atomic radii and number of d electrons affecting p - d orbital hybridizations vary with the type of TM element, it is reasonable to appear of plentiful stable phases for the TM monolayers on Gy, depending not only on the group index but also on the period index. Note that all the monolayers of TM with 6 d electrons, i.e., Ni, Pd, Pt, present the NM phase, because the hybridization with p orbitals of C makes d orbitals completely filled.

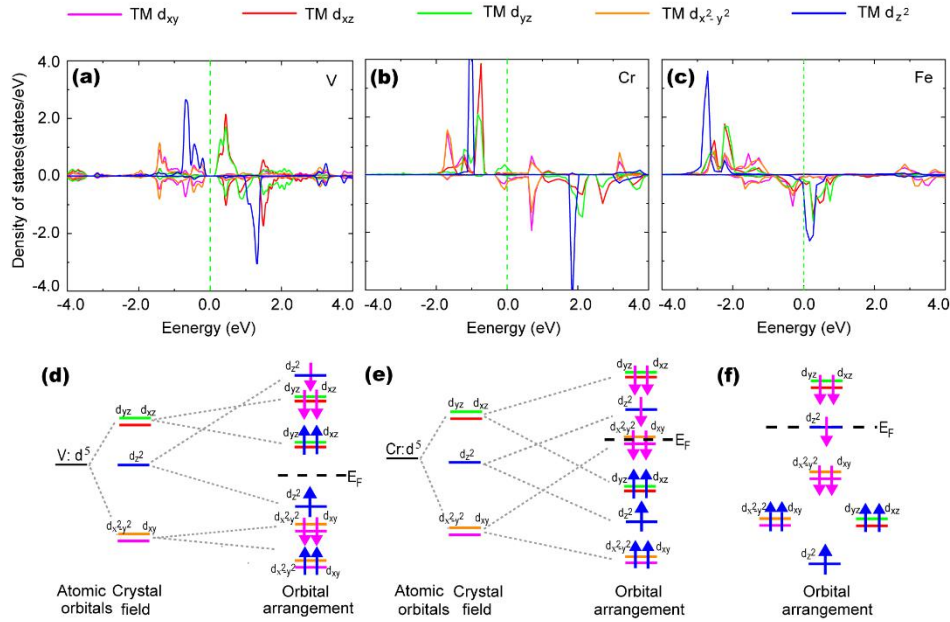


Figure 2. (Color online) The calculated PDOS and d orbital arrangement of a single TM atom in the Gy/TM system. The d -orbital PDOS (a) and orbital arrangement (d) of a V atom in Gy/V with larger atomic radius ($\geq 1.34\text{\AA}$). The orbital arrangement characteristics for Gy/TM with TM=Cr, Mn, Te, Ta, Re are similar to Gy/V. (b)(c) and (e)(f) are the results for systems with smaller atomic radius ($< 1.30\text{\AA}$). Note that Gy/Co has similar orbital arrangement with Gy/Cr, and Gy/Mn has similar orbital arrangement with Gy/Fe. The red and green lines, the blue lines, the magenta and orange lines represent degenerate $d_{x^2-y^2}/d_{xy}$ orbitals, single d_{z^2} orbitals, degenerate d_{xz}/d_{yz} orbitals, respectively. E_F is Fermi level. The split of energy levels of d orbitals (except for Fe and Mn as discussed in the text) basically present a TPCF-like distribution.

Then we focus on the 11 TM monolayers which have the strong FM or AFM ground states with larger magnetic momentum ($> 0.5\ \mu_B/\text{atom}$). As shown in Figure 1b, 5 of 11 (Fe, Co, Nb, Mo, W) TM elements present the strong FM ground state, and the remaining 6 (V, Cr, Mn, Te, Ta, Re) have the strong AFM ground state. The PDOS calculations show that these ground states

can be described by three kinds of orbital arrangement (Figure 2d-f). The first two are originated from the TPCF-like filed, that is, the TM elements with atomic radius larger than 1.34 Å (V, Nb, Ta, Mo, W, Tc, Re) have d_{z^2} and d_{xz}/d_{yz} orbitals locating on the VBM and CBM respectively, whereas those with atomic radius smaller than 1.30 Å (Cr, Co) mainly have $d_{x^2-y^2}/d_{xy}$ orbitals nearby E_F . The third kind is for Fe and Mn which also have small atomic radius (1.26 Å and 1.27 Å). While, the exchange field presents complex orbital arrangement with degenerated $d_{x^2-y^2}/d_{xy}$ and d_{xz}/d_{yz} orbitals as shown in Figure 2f, which cannot be directly derived from the TPCF-like filed. These results show that the exchange field of TM monolayer is induced by the combined effect of atomic radii (more dominating) and number of d valance electrons of the TM element.

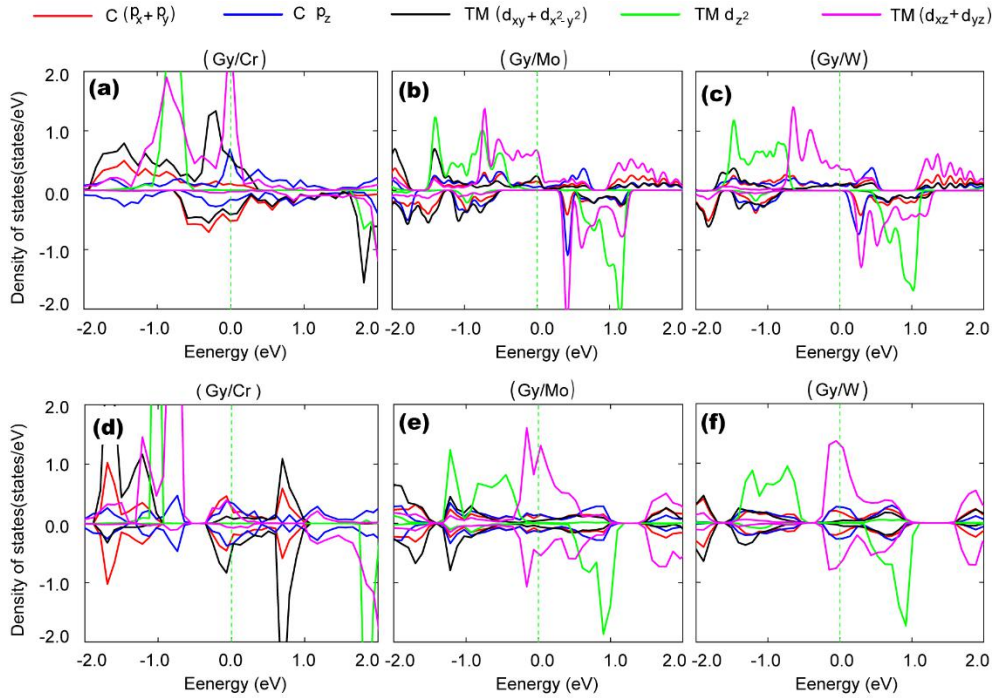


Figure 3. (Color online) The calculated PDOS of Gy/TM. (a), (b) and (c) represent the PDOS of magnetic systems of Gy/TM(TM=Cr, Mo, W). (d), (e) and (f) represent the PDOS of antiferromagnetic systems of them, respectively. The red (for degenerate p_x/p_x orbital) and blue (for p_z orbital) lines represent the PDOS of the six C nearest to TM, respectively. Black lines represent the degenerate $d_{x^2-y^2}/d_{xy}$ orbitals, magenta lines represent the degenerate d_{xz}/d_{yz} orbitals, and green lines represent the d_{z^2} orbitals of TM, respectively. The competition between the super-exchange induced by the hybridization of $p-d$ orbitals and the direct exchange induced by the overlaps between the $d-d$ orbitals determines the magnetic ground state of the systems. The PDOS of d orbitals are from one TM atom of the unit cell.

Based on the detailed analysis of PDOS, we found that the ground FM/AFM magnetic state is attributed to the competition between direct exchange and super-exchange of d electrons. In the following, we show the details by taking Cr, Mo, W in group VI B as an example. We firstly considered Cr monolayer, which has an AFM ground state. [Figure 3a](#) and [3d](#) show the PDOS of a Cr atom in the FM and AFM phases, respectively. It is shown that there are obvious overlaps of PDOS peaks for p_x/p_y and $d_{x^2-y^2}/d_{xy}$, as well as for p_z and d_{xz}/d_{yz} orbitals, indicating the significant p - d orbital hybridizations. Such orbital hybridizations are expected to induce strong super-exchange magnetic interactions contributing to the AFM phase, between two nearest Cr atoms bridged by the two bonded C atoms ([Figure 1](#)). On the other hand, there are also direct d - d orbital overlaps between two nearest-neighbor Cr atoms, contributing to the FM phase. Therefore, the magnetic ground state is determined by the competition between the super-exchange and direct exchange effects, where the super-exchange effect is dominant for Cr monolayer. Note that the direct exchange effect would be dominant for Mo and W monolayers, because the p - d orbital hybridizations contributing to the AFM phase become weaker, whereas the direct d - d orbital overlaps become stronger due to the increase of atomic radii. This feature is confirmed by the calculated PDOS of a Mo (W) atom shown in [Figure 3b](#) and [3e](#) ([Figure 3c](#) and [3f](#)) with both FM and AFM phases, where the overlapped peaks of p - d orbitals become obviously smaller but the width of d orbital DOS nearby Fermi level gets much larger compared to that of Cr.

Now we come to discuss the electronic properties of Gy/TM. As shown in [Figure 1b](#) and [Figure S3](#), the TM monolayers exhibit plentiful electronic properties, including metal, semiconductor, as well as semimetal. Here we focus on the TM monolayers with FM ground state, which may have potential applications in the spintronics. [Figure 4](#) shows the calculated band structures of Nb, Mo, and W monolayers on Gy, which exhibit either half-metal or half-semiconductor characteristics distinguished from their bulk phases. As shown in the [figure 4](#), Mo and W monolayers are ideal half-metals with pure spin-up electrons appearing in $[-0.5, 0.4]$ eV and $[-0.8, 0.1]$ eV, respectively. Whereas, Nb monolayer exhibits half-semiconductor characteristic with energy gap of 0.1 eV, where the pure spin-up electrons appears in $[-0.5, 0.2]$ eV. On the other hand, although the Fe and Co monolayers do not have half-metal characteristic,

they still have pure spin-down electrons nearby the Fermi level, i.e., $[-0.2, -1.0]$ eV and $[-0.3, -0.7]$ eV, respectively (Figure S2). This feature shows these TM monolayers can be ideal materials for the spin transport devices.

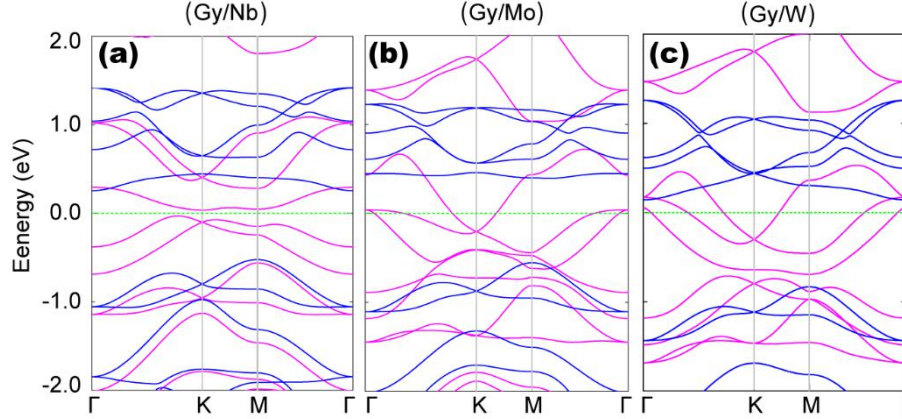


Figure 4. (Color online) Half-metallic Gy/TM system. (a), (b), and (c) respectively represent the half-metal system of Gy/TM(TM=Nb, Mo, W). Magenta and blue represent the spin-up and spin-down electronic states, respectively. Gy/Nb exhibits half-semiconductor characteristic with energy gap of 0.1 eV, where the pure spin-up electrons appears in $[-0.5, 0.2]$ eV. Mo and W systems are half-metals with pure spin-up electrons appearing in $[-0.5, 0.4]$ eV and $[-0.8, 0.1]$ eV, respectively.

To verify the application potentials of TM monolayers in the spintronic devices, we further explored the TMR of a horizontal MTJ device based on the Gy/TM structure (Figure 5a). It is known that the vertical MTJ devices based on 2D materials have been widely studied in the past decade, however, the investigation on horizontal MTJ is still scarce due to the difficulty in realizing the 2D horizontal magnetic heterostructures in experiments. Here we propose that one can realize the horizontal MTJ device much easier in the use of the Gy/TM system, i.e., deposit different TM atoms using the MASK method to make magnetic layers, and leave undeposited region (bare Gy) as the tunneling layer since Gy is a semiconductor with band gap about 0.4 eV.⁶⁴ We further show a horizontal MTJ device model in Figure 5a, where the source and drain electrodes are composed of Gy/Mo, and the free magnetic layer and tunneling layer are composed by Gy/W and bare Gy, respectively. The parallel (P) and anti-parallel (AP) magnetization states of the MTJ are realized by flipping the magnetization direction of W monolayer as indicated in Figure 5b. The calculated transmission spectrum of the P and AP

states for different spins with zero bias are shown in Figure 5c. As one can see, in both cases the spin-up (T_{\uparrow}) electron transmission is larger than that of spin-down (T_{\downarrow}) electrons nearby the Fermi level by about ten orders, manifesting a perfect spin-filtering effect. We further evaluated the TMR of the MTJ, which is defined as $|(T_P - T_{AP})/T_{AP}| \times 100\%$, with $T_P = T_{\uparrow} + T_{\downarrow}$ and $T_{AP} = T_{\uparrow} + T_{\downarrow}$, respectively. As shown in Figure 5d, the 2D device has exceptionally TMR of about 2800% at the Fermi level and 850000% at -0.63eV, respectively. Especially, the 850000% is significantly larger than the reported record realized in the vertical MTJ based on multilayer CrI_3 (57000%).⁶⁵ This feature confirms the great application potentials of Gy/TM horizontal MTJ devices in future spintronic devices.

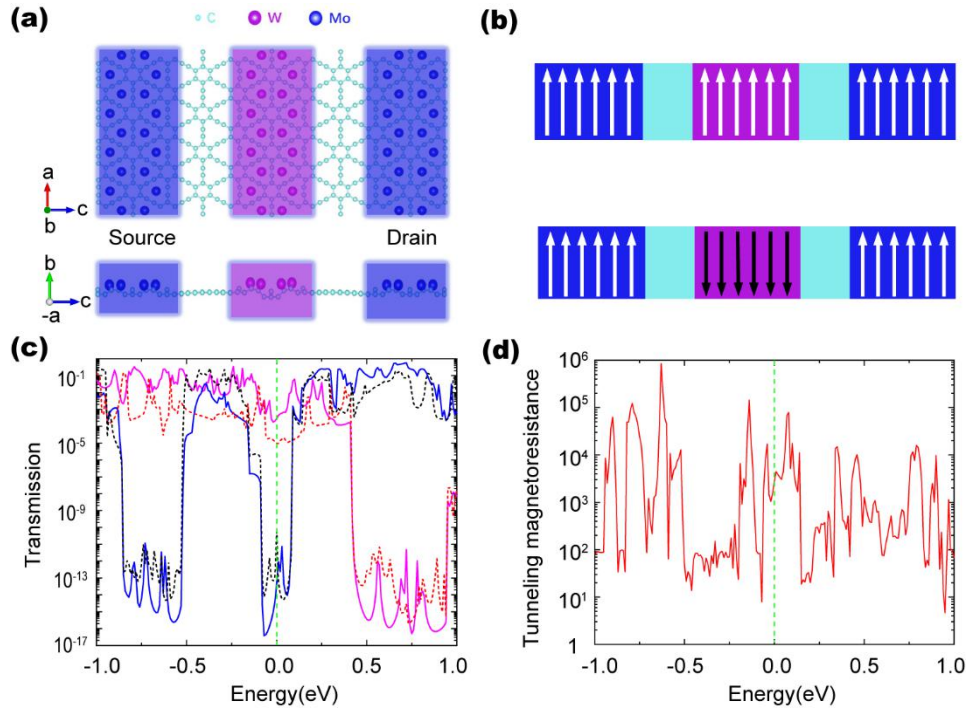


Figure 5. (Color online) Gy/TM horizontal MTJ device model and calculated electronic transport properties. (a) MTJ device model in top view (upper panel) and side view (lower panel). (b) Schematic diagram of the magnetic sequence of the device changing from a parallel (P) state to an anti-parallel (AP) state. (c) Calculated transmission spectra of the P state and AP state under zero bias. The solid line and the dashed line represent the device configuration in the P and AP states, respectively. The magenta (red) and blue (black) solid lines represent the transmission for spin up and spin down states, respectively. (d) Calculated tunneling magnetoresistance as a function of energy level.

In summary, by using the first-principles calculations we have proposed a new approach to obtain monolayer TM magnets, i.e., depositing TM atoms on substrate with hexagonal hollow

geometry. We have demonstrated the feasibility of this approach on Gy substrate, where the TM monolayer with perfect hexagonal geometry has been formed. We have also found the TM monolayer exhibits a wealth of physical properties, including FM and AFM ground states, as well as semimetal and half-metal characteristics. The competition between direct exchange and super-exchange interactions have been proposed to explain the variation of magnetic phases. Finally, we have demonstrated the TM monolayers have great potential applications in the spintronics, where the TMR in the horizontal MTJ device model is calculated to be 2800% at the Fermi level and as high as 850000% at -0.63eV, respectively.

ASSOCIATED CONTENT

Supporting Information.

The following files are available free of charge.

The structure and physical properties of systems Gy/TM; Band projection of Gy/TM system; The band structures of the Gy/Fe and Gy/Co; Band structure of Gy/TM in different ground states.

AUTHOR INFORMATION

Corresponding Author

* E-mail Present Addresses: zxguo08@xjtu.edu.cn

ACKNOWLEDGMENT

We are grateful for useful discussions with Dr. Lei Wang and Dr. Yongliang Shi. This work is supported by the National Natural Science Foundation of China (No. 12074301 and No. 12004295), National Key R&D Program of China (2018YFB0407600), Science Fund for Distinguished Young Scholars of Hunan Province (No. 2018JJ1022), Fundamental Research Funds for Central Universities (No. xzy012019062), and Open Research Fund of Key Laboratory

of Polar Materials and Devices, Ministry of Education. P.L. thanks China's Postdoctoral Science Foundation funded project (NO. 2020M673364).

ABBREVIATIONS

Gy, Graphyne; TM, Transition Metal; MTJ, Magnetic Tunnel Junction; TMR, Tunneling magnetoresistance; TPCF, Triangular-prism-crystal-field

REFERENCES

- (1) Wang, Z.; Ki, D. K.; Chen, H.; Berger, H.; MacDonald, A. H.; Morpurgo, A. F., Strong interface-induced spin-orbit interaction in graphene on WS₂. *Nat. Commun.* **2015**, *6* (1), 1-7.
- (2) Han, W., Perspectives for spintronics in 2D materials. *APL Mater.* **2016**, *4* (3), 032401.
- (3) Feng, Y. P.; Shen, L.; Yang, M.; Wang, A.; Zeng, M.; Wu, Q.; Chintalapati, S.; Chang, C. R., Prospects of spintronics based on 2D materials. *Wiley Interdiscip. Rev.: Comput. Mol. Sci.* **2017**, *7* (5), e1313.
- (4) Kim, H. H.; Yang, B.; Patel, T.; Sfigakis, F.; Li, C.; Tian, S.; Lei, H.; Tsen, A. W., One million percent tunnel magnetoresistance in a magnetic van der Waals heterostructure. *Nano Lett.* **2018**, *18* (8), 4885-4890.
- (5) Xie, Q.; Lin, W.; Yang, B.; Shu, X.; Chen, S.; Liu, L.; Yu, X.; Breese, M. B.; Zhou, T.; Yang, M., Giant enhancements of perpendicular magnetic anisotropy and spin-orbit torque by a MoS₂ layer. *Adv. Mater.* **2019**, *31* (21), 1900776.
- (6) Yazyev, O. V.; Helm, L., Defect-induced magnetism in graphene. *Phys. Rev. B* **2007**, *75* (12), 125408.
- (7) Nair, R.; Sepioni, M.; Tsai, I.-L.; Lehtinen, O.; Keinonen, J.; Krasheninnikov, A.; Thomson, T.; Geim, A.; Grigorieva, I., Spin-half paramagnetism in graphene induced by point defects. *Nat. Phys.* **2012**, *8* (3), 199-202.
- (8) Han, W.; Kawakami, R. K.; Gmitra, M.; Fabian, J., Graphene spintronics. *Nat. Nanotechnol.* **2014**, *9* (10), 794-807.
- (9) Červenka, J.; Katsnelson, M.; Flipse, C., Room-temperature ferromagnetism in graphite driven by two-dimensional networks of point defects. *Nat. Phys.* **2009**, *5* (11), 840-844.
- (10) McCreary, K. M.; Swartz, A. G.; Han, W.; Fabian, J.; Kawakami, R. K., Magnetic moment formation in graphene detected by scattering of pure spin currents. *Phys. Rev. Lett.* **2012**, *109* (18), 186604.
- (11) Giesbers, A.; Uhlířová, K.; Konečný, M.; Peters, E.; Burghard, M.; Aarts, J.; Flipse, C., Interface-induced room-temperature ferromagnetism in hydrogenated epitaxial graphene. *Phys. Rev. Lett.* **2013**, *111* (16), 166101.
- (12) Boukhvalov, D.; Katsnelson, M.; Lichtenstein, A., Hydrogen on graphene: Electronic structure, total energy, structural distortions and magnetism from first-principles calculations. *Phys. Rev. B* **2008**, *77* (3), 035427.
- (13) Yazyev, O. V.; Katsnelson, M., Magnetic correlations at graphene edges: basis for novel spintronics devices. *Phys. Rev. Lett.* **2008**, *100* (4), 047209.

- (14) Jung, J.; Pereg-Barnea, T.; MacDonald, A., Theory of interedge superexchange in zigzag edge magnetism. *Phys. Rev. Lett.* **2009**, *102* (22), 227205.
- (15) Son, Y.-W.; Cohen, M. L.; Louie, S. G., Half-metallic graphene nanoribbons. *Nature* **2006**, *444* (7117), 347-349.
- (16) Stauber, T.; Peres, N.; Guinea, F.; Neto, A. C., Fermi liquid theory of a Fermi ring. *Phys. Rev. B* **2007**, *75* (11), 115425.
- (17) Castro, E. V.; Peres, N.; Stauber, T.; Silva, N., Low-density ferromagnetism in biased bilayer graphene. *Phys. Rev. Lett.* **2008**, *100* (18), 186803.
- (18) Maryenko, D.; Mishchenko, A.; Bahramy, M.; Ernst, A.; Falson, J.; Kozuka, Y.; Tsukazaki, A.; Nagaosa, N.; Kawasaki, M., Observation of anomalous Hall effect in a non-magnetic two-dimensional electron system. *Nat. Commun.* **2017**, *8* (1), 1-7.
- (19) Deng, Y.; Yu, Y.; Song, Y.; Zhang, J.; Wang, N. Z.; Sun, Z.; Yi, Y.; Wu, Y. Z.; Wu, S.; Zhu, J., Gate-tunable room-temperature ferromagnetism in two-dimensional Fe₃GeTe₂. *Nature* **2018**, *563* (7729), 94-99.
- (20) Li, P.; Ma, Y.; Zhang, Y.; Guo, Z.-X., Room Temperature Quantum Anomalous Hall Insulator in a Honeycomb-Kagome Lattice, Ta₂O₃, with Huge Magnetic Anisotropy Energy. *ACS Appl. Electron. Mater.* **2021**.
- (21) Li, P.; Cai, T.-Y., Fully spin-polarized quadratic non-Dirac bands realized quantum anomalous Hall effect. *Phys. Chem. Chem. Phys.* **2020**, *22* (2), 549-555.
- (22) Parkin, S.; More, N.; Roche, K., Oscillations in exchange coupling and magnetoresistance in metallic superlattice structures: Co/Ru, Co/Cr, and Fe/Cr. *Phys. Rev. Lett.* **1990**, *64* (19), 2304.
- (23) Lado, J. L.; Fernández-Rossier, J., On the origin of magnetic anisotropy in two dimensional CrI₃. *2D Mater.* **2017**, *4* (3), 035002.
- (24) Binasch, G.; Grünberg, P.; Saurenbach, F.; Zinn, W., Enhanced magnetoresistance in layered magnetic structures with antiferromagnetic interlayer exchange. *Phys. Rev. B* **1989**, *39* (7), 4828.
- (25) Huang, B.; Clark, G.; Navarro-Moratalla, E.; Klein, D. R.; Cheng, R.; Seyler, K. L.; Zhong, D.; Schmidgall, E.; McGuire, M. A.; Cobden, D. H., Layer-dependent ferromagnetism in a van der Waals crystal down to the monolayer limit. *Nature* **2017**, *546* (7657), 270-273.
- (26) Li, J.; Li, Y.; Du, S.; Wang, Z.; Gu, B.-L.; Zhang, S.-C.; He, K.; Duan, W.; Xu, Y., Intrinsic magnetic topological insulators in van der Waals layered MnBi₂Te₄-family materials. *Sci. Adv.* **2019**, *5* (6), eaaw5685.
- (27) Otrokov, M. M.; Klimovskikh, I. I.; Bentmann, H.; Zeugner, A.; Aliev, Z. S.; Gass, S.; Wolter, A. U.; Koroleva, A. V.; Estyunin, D.; Shikin, A. M., Prediction and observation of the first antiferromagnetic topological insulator. *arXiv preprint arXiv:1809.07389* **2018**.
- (28) Gong, C.; Li, L.; Li, Z.; Ji, H.; Stern, A.; Xia, Y.; Cao, T.; Bao, W.; Wang, C.; Wang, Y., Discovery of intrinsic ferromagnetism in two-dimensional van der Waals crystals. *Nature* **2017**, *546* (7657), 265-269.
- (29) Zhou, W.; Zou, X.; Najmaei, S.; Liu, Z.; Shi, Y.; Kong, J.; Lou, J.; Ajayan, P. M.; Yakobson, B. I.; Idrobo, J.-C., Intrinsic structural defects in monolayer molybdenum disulfide. *Nano Lett.* **2013**, *13* (6), 2615-2622.
- (30) Banhart, F.; Kotakoski, J.; Krasheninnikov, A. V., Structural defects in graphene. *ACS Nano* **2011**, *5* (1), 26-41.
- (31) Lin, Z.; McCreary, A.; Briggs, N.; Subramanian, S.; Zhang, K.; Sun, Y.; Li, X.; Borys, N. J.; Yuan, H.; Fullerton-Shirey, S. K., 2D materials advances: from large scale synthesis and

- controlled heterostructures to improved characterization techniques, defects and applications. *2D Mater.* **2016**, *3* (4), 042001.
- (32) Zheng, Y. J.; Chen, Y.; Huang, Y. L.; Gogoi, P. K.; Li, M.-Y.; Li, L.-J.; Trevisanutto, P. E.; Wang, Q.; Pennycook, S. J.; Wee, A. T., Point defects and localized excitons in 2D WSe₂. *ACS Nano* **2019**, *13* (5), 6050-6059.
- (33) Ikeda, S.; Hayakawa, J.; Lee, Y. M.; Matsukura, F.; Ohno, Y.; Hanyu, T.; Ohno, H., Magnetic tunnel junctions for spintronic memories and beyond. *IEEE Trans. Electron Devices* **2007**, *54* (5), 991-1002.
- (34) Sato, K.; Katayama-Yoshida, H., First principles materials design for semiconductor spintronics. *Semicond. Sci. Technol.* **2002**, *17* (4), 367.
- (35) Ghosh, S.; Choubey, C.; Sil, A., Photocatalytic response of Fe, Co, Ni doped ZnO based diluted magnetic semiconductors for spintronics applications. *Superlattices Microstruct.* **2019**, *125*, 271-280.
- (36) Xu, C.; Wang, L.; Liu, Z.; Chen, L.; Guo, J.; Kang, N.; Ma, X.-L.; Cheng, H.-M.; Ren, W., Large-area high-quality 2D ultrathin Mo₂C superconducting crystals. *Nat. Mater.* **2015**, *14* (11), 1135-1141.
- (37) Novoselov, K. S.; Geim, A. K.; Morozov, S. V.; Jiang, D.; Zhang, Y.; Dubonos, S. V.; Grigorieva, I. V.; Firsov, A. A., Electric field effect in atomically thin carbon films. *Science* **2004**, *306* (5696), 666-669.
- (38) Verger, L.; Xu, C.; Natu, V.; Cheng, H.-M.; Ren, W.; Barsoum, M. W., Overview of the synthesis of MXenes and other ultrathin 2D transition metal carbides and nitrides. *Curr. Opin. Solid State Mater. Sci.* **2019**, *23* (3), 149-163.
- (39) Goryunov, Y. V.; Garif'yanov, N.; Khaliullin, G.; Garifullin, I.; Tagirov, L.; Schreiber, F.; Mühge, T.; Zabel, H., Magnetic anisotropies of sputtered Fe films on MgO substrates. *Phys. Rev. B* **1995**, *52* (18), 13450.
- (40) Xu, Y.; Kernohan, E.; Freeland, D.; Ercole, A.; Tselepi, M.; Bland, J., Evolution of the ferromagnetic phase of ultrathin Fe films grown on GaAs (100)-4×6. *Phys. Rev. B* **1998**, *58* (2), 890.
- (41) Kresse, G.; Furthmüller, J., Efficient iterative schemes for ab initio total-energy calculations using a plane-wave basis set. *Phys. Rev. B* **1996**, *54* (16), 11169.
- (42) Kresse, G.; Hafner, J., Ab initio molecular dynamics for liquid metals. *Phys. Rev. B* **1993**, *47* (1), 558.
- (43) Kresse, G.; Joubert, D., From ultrasoft pseudopotentials to the projector augmented-wave method. *Phys. Rev. B* **1999**, *59* (3), 1758.
- (44) Blöchl, P. E., Projector augmented-wave method. *Phys. Rev. B* **1994**, *50* (24), 17953.
- (45) Monkhorst, H. J.; Pack, J. D., Special points for Brillouin-zone integrations. *Phys. Rev. B* **1976**, *13* (12), 5188.
- (46) Jelver, L.; Larsen, P. M.; Stradi, D.; Stokbro, K.; Jacobsen, K. W., Determination of low-strain interfaces via geometric matching. *Phys. Rev. B* **2017**, *96* (8), 085306.
- (47) Brandbyge, M.; Mozos, J.-L.; Ordejón, P.; Taylor, J.; Stokbro, K., Density-functional method for nonequilibrium electron transport. *Phys. Rev. B* **2002**, *65* (16), 165401.
- (48) Soler, J. M.; Artacho, E.; Gale, J. D.; García, A.; Junquera, J.; Ordejón, P.; Sánchez-Portal, D., The SIESTA method for ab initio order-N materials simulation. *J. Phys.: Condens. Matter* **2002**, *14* (11), 2745.
- (49) Taylor, J.; Guo, H.; Wang, J., Ab initio modeling of quantum transport properties of molecular electronic devices. *Phys. Rev. B* **2001**, *63* (24), 245407.

- (50) Grimme, S.; Antony, J.; Ehrlich, S.; Krieg, H., A consistent and accurate ab initio parametrization of density functional dispersion correction (DFT-D) for the 94 elements H-Pu. *J Chem Phys* **2010**, *132* (15), 154104.
- (51) Grimme, S.; Ehrlich, S.; Goerigk, L., Effect of the damping function in dispersion corrected density functional theory. *J. Comput. Chem.* **2011**, *32* (7), 1456-1465.
- (52) Li, Q.; Li, Y.; Chen, Y.; Wu, L.; Yang, C.; Cui, X., Synthesis of γ -graphyne by mechanochemistry and its electronic structure. *Carbon* **2018**, *136*, 248-254.
- (53) Kang, J.; Li, J.; Wu, F.; Li, S.-S.; Xia, J.-B., Elastic, electronic, and optical properties of two-dimensional graphyne sheet. *J. Phys. Chem. C* **2011**, *115* (42), 20466-20470.
- (54) Pan, L.; Zhang, L.; Song, B.; Du, S.; Gao, H.-J., Graphyne-and graphdiyne-based nanoribbons: density functional theory calculations of electronic structures. *Appl. Phys. Lett.* **2011**, *98* (17), 173102.
- (55) Narita, N.; Nagai, S.; Suzuki, S.; Nakao, K., Optimized geometries and electronic structures of graphyne and its family. *Phys. Rev. B* **1998**, *58* (16), 11009.
- (56) Li, G.; Li, Y.; Liu, H.; Guo, Y.; Li, Y.; Zhu, D., Architecture of graphdiyne nanoscale films. *Chem. Commun.* **2010**, *46* (19), 3256-3258.
- (57) Jiao, Y.; Du, A.; Hankel, M.; Zhu, Z.; Rudolph, V.; Smith, S. C., Graphdiyne: a versatile nanomaterial for electronics and hydrogen purification. *Chem. Commun.* **2011**, *47* (43), 11843-11845.
- (58) Srinivasu, K.; Ghosh, S. K., Graphyne and graphdiyne: promising materials for nanoelectronics and energy storage applications. *J. Phys. Chem. C* **2012**, *116* (9), 5951-5956.
- (59) Li, P.; Li, X.; Zhao, W.; Chen, H.; Chen, M.-X.; Guo, Z.-X.; Feng, J.; Gong, X.-G.; MacDonald, A. H., Topological Dirac states beyond π -orbitals for silicene on SiC (0001) surface. *Nano Lett.* **2017**, *17* (10), 6195-6202.
- (60) Li, L.; Wang, Y.; Xie, S.; Li, X.-B.; Wang, Y.-Q.; Wu, R.; Sun, H.; Zhang, S.; Gao, H.-J., Two-dimensional transition metal honeycomb realized: Hf on Ir (111). *Nano Lett.* **2013**, *13* (10), 4671-4674.
- (61) Zhao, J.; Liu, H.; Yu, Z.; Quhe, R.; Zhou, S.; Wang, Y.; Liu, C. C.; Zhong, H.; Han, N.; Lu, J., Rise of silicene: A competitive 2D material. *Prog. Mater. Sci.* **2016**, *83*, 24-151.
- (62) Oughaddou, H.; Enriquez, H.; Tchalala, M. R.; Yildirim, H.; Mayne, A. J.; Bendounan, A.; Dujardin, G.; Ali, M. A.; Kara, A., Silicene, a promising new 2D material. *Prog. Surf. Sci.* **2015**, *90* (1), 46-83.
- (63) Wang, K.; Zhang, Y.; Zhao, W.; Li, P.; Ding, J.-W.; Xie, G.-F.; Guo, Z.-X., Topological Dirac states in transition-metal monolayers on graphyne. *Phys. Chem. Chem. Phys.* **2019**, *21* (18), 9310-9316.
- (64) Puigdollers, A. R.; Alonso, G.; Gamallo, P., First-principles study of structural, elastic and electronic properties of α -, β -and γ -graphyne. *Carbon* **2016**, *96*, 879-887.
- (65) Song, T.; Tu, M. W.-Y.; Carnahan, C.; Cai, X.; Taniguchi, T.; Watanabe, K.; McGuire, M. A.; Cobden, D. H.; Xiao, D.; Yao, W., Voltage control of a van der Waals spin-filter magnetic tunnel junction. *Nano Lett.* **2019**, *19* (2), 915-920.